Orbital Interpretation of Kinetic Energy Density and a Direct Space Comparison of Chemical Bonding in Tetrahedral Network Solids

Dong-Kyun Seo* and Chang'e Weng

Department of Chemistry and Biochemistry, Arizona State University, Tempe, Arizona 85287-1604

Received: April 15, 2008; Revised Manuscript Received: May 17, 2008

We present how the kinetic energy density (KED) can be interpreted on the basis of the orbital interactions within the Kohn−Sham theory and propose how to utilize a direct space function in chemical bonding analysis, the relative entropy density (RED), which is constructed from the KED, the Thomas−Fermi KED (TF-KED), and the electron density. From the detailed analysis of the KED of wave functions and the TF-KED from the free electron model, it is shown that the RED can reveal the nodal properties of individual wave functions and provide a variationally meaningful way of accumulating chemical bonding information from the wave functions, hence allowing quantitative bonding analysis in direct space. To substantiate the proposal, the RED function has been tested on the tetrahedral network solids, including the group 14 elements and the III−V binary compounds with the zinc blende structure. The direct space maps of the RED quantitatively reflect the trend in metallicity and the polarity of their two-center, two-electron bonds in terms of the absolute values of the RED, the location of the minimum values, and the behavior of the deformation from the spherical symmetry of the atomic RED.

Introduction

The investigation of the chemical bonding properties of solids is often nontrivial and requires multiple approaches, especially for relatively covalent solids including metals.[1] The problem escalates drastically as the constituent elements become heavier and the catenation patterns become more complicated. Not to mention a required expertise in electronic band structure calculations and a comprehensive understanding of various chemical bonding types, a detailed analysis of almost an infinite number of wave functions (crystal orbitals) is overwhelming without any simplifying analytical tools.

The analysis of electronic band structure based on the crystal orbital overlap population (COOP)[2] or the crystal orbital Hamilton population (COHP)[3] is useful in that sense because it does not require a thorough understanding of the reciprocal space; it extracts bonding information from the wave functions through an integration in the reciprocal space and in the direct space and subsequently presents it as pairwise atomic (or orbital) interactions spanning along the one-electron energy axis. The strength of covalent bonding between a pair of atoms can be estimated by the integration of the overlap populations up to the Fermi energy. Therefore, the orbital overlap population analysis correlates the bonding/antibonding characteristics of the wave functions with their energies. Because it projects any interatomic interactions into atomic pair interactions, however, the distinction in bonding character is given through the differences in the COOP or the COHP values between atom pairs, even when the bonding is well delocalized among multicenters or very polarized among different types of atoms. In addition, the method is limited to calculation methods that are based on atomic orbitals.

Direct space methods take an alternative approach that emphasizes the spatial variation of bonding descriptors such as the electron density (or its gradient),[4] the electron localization function (ELF),[5] the electron localization index (ELI),[6] and the localized-orbital locator (LOL),[7] which are not restricted to specific calculation methods. A 3-D visualization of the chemical bonding can be attractive because it may provide an instant view of the bonding characteristics presented directly in the frame of crystal structures. Whereas the electron density gradient method is designed to find bonding paths in chemical structures by utilizing electron density maps from either calculations or measurements, the ELF (and the ELI) and the LOL focus on locating electron pairs and domains of localized orbitals, respectively, by employing various kinds of kinetic energy densities of electrons as basic components, namely, the positive kinetic energy density (KED), the Thomas−Fermi kinetic energy density (TF-KED), and the von Weizsäcker kinetic energy density (W-KED).

In fact, a more fundamental significance of the KED lies in Ruedenberg's recognition that a lowering of the kinetic energy in the bonding region is considered to be the physical origin of covalent bonding.[8] Over the following several decades, the role of kinetic energy (the spatial distribution of kinetic energy, in a precise sense) in bonding formation has been studied thoroughly via ab initio calculations of small molecules.[9] However, the KED is also significant in the density functional theory because important breakthroughs in its advances have been made through detailed investigations of the nature of the KED in terms of the exchange-correlation effect.[10] More closely related to this work, the KED from the Kohn−Sham calculations has been examined in the bonding analysis through its connection to the off-diagonal elements in the spin-traced reduced, one-particle density matrix (one-matrix)[7b] and also in the chemical reactivity analysis through the thermodynamic description of density functional theory.[11]

More recently, a variational meaning of the KED has been established within local density functional theory.[12] That is, when relative entropy is defined as the measure of the information deviation of the KED from the TF-KED, the condition that produces a minimum energy should result in a maximum value of the relative entropy (or the entropy functional itself; see later

* Corresponding author. E-mail: dseo@asu.edu.

10.1021/jp803279e CCC: $40.75
Published on Web 07/31/2008

sections).[13] Given the fact that the Thomas−Fermi model does not allow chemical bond formation (Teller's molecular nonbinding theorem),[14] the KED may exhibit chemical bonding information when it is compared with the TF-KED through the definition of the relative entropy.

Despite the recurrent role of the KED in quantum chemical and density functional theories, its meaning in view of orbital interactions has been missing in the literature. An eminent value of such an approach is the connection of the electronic structure to the chemical bonding concept and the establishment of a conceptual framework that is consistent with molecular orbital (MO) theory through the analysis of many-electron states in terms of the component one-electron energy levels. The work closest to this notion is that by Burdett, who found that the results obtained by the study of ELF maps are usually independent of whether the wave functions and electron density were generated by calculations that included electron−electron interactions (such as ab initio and first principle calculations) or those that did not (extended Hückel calculations, for example).[5d] This is in accord with the general ideas of chemical bonding; the essence of the picture may often be gained simply from orbital overlap and electronegativity (EN) considerations. It has been further concluded that the formal inclusion of electron−electron interactions usually changes the bonding picture only a little in the ELF maps.[5d]

The concept of the relative entropy is useful in that sense because we shall see progressively throughout this work that, at least within Kohn−Sham theory, it provides a solid justification for the use of the KED for the orbital analysis based on the variation principle. As demonstrated previously, the Kohn−Sham orbitals are physically sound and may be expected to be quite suitable for use in qualitative (or even semiquantitative) MO theory.[15] Our recent studies have extended such a viewpoint to the studies of magnetic interactions in molecules and solids.[16]

Herein, we first show that the wave function expression of the KED indeed contains the orbital interaction information, and we subsequently examine the plausibility of the applications of the relative entropy density (an unintegrated form of relative entropy) in the investigation of chemical bonding in some tetrahedral network solids. Whereas more examples will follow in our subsequent studies, we note that the tetrahedral network solids represented by the group 14 elements and the III−V zinc blende compounds are an ideal starting point in the investigation of chemical bonding character. Although all of these solids are understood on the basis of two-center two-electron bonds, the metallicity of the bonds increases as the constituent elements become heavier, and the bond polarity changes significantly depending on the atomic pair combinations. By comparing bonds of the same structural type it is possible to identify the essential similarities and differences among different bonding types. We reiterate that the close-packing structures of metals or ionic compounds are a consequence rather than the origin of the nondirectional nature of the metallic or ionic bonds. As an additional benefit, the tetrahedral network solids have been studied by other direct-space methods, particularly the ELF,[5e] which allows a comparison of our new method with others.

Calculation Methods

The algebraic calculations and the analysis of the direct-space functions were carried out by utilizing Mathematica 6 and its graphics utilities. The numerical calculations were performed by implementing the calculation routines in D-Grid 3.1[17] and in the VASP[18] programs. The modified D-Grid allows for calculations of the direct space functions for molecules by using the calculation results of the Gaussian 03[19] package employed in molecules. The results from the D-Grid 3.1 and VASP calculations were visualized with the XCrysDen program.[20]

All VASP calculations were carried out by using the projector augmented wave (PAW) potentials[21] with a generalized gradient approximation (GGA).[22] A plane wave cutoff of 300 eV was used for C in the diamond structure and for BN in the zinc blende structure with their reduced two-atom unit cells. For the other group 14 elements and III−V compounds, a plane wave cutoff of 240 eV was used. For all of the solids, the unit cell parameters were obtained from the literature. A k-point grid density of $11 \times 11 \times 11$ was used for all of the solids. For isolated atoms, a unit cell of $15 \times 15 \times 15$ Å^3 was used with default energy cutoffs from 100 to 400 eV (energy cutoffs of 400, 245, 174, and 103 eV for C, Si, Ge, and Sn, respectively). An H_2 molecule was contained in a unit cell of $10 \times 10 \times 10$ Å^3, and a plane wave cutoff of 400 eV was used.

With the density functional code in the Gaussian 03 program, all of the geometries of the molecules were optimized at the B3LYP/LANL2DZ level where the Becke three-parameter hybrid functional[23] and the Lee−Yang−Parr correlation functional[24] were used. Geometries were restricted to tetrahedral symmetry for the central atom in order to simulate the tetrahedral bonds in the crystal structures. In the LANL2DZ basis set,[25] the Dunning−Huzinaga valence double-ς was employed in the elements of the first and second periods (all-electron, full-potential), and Los Alamos effective core potentials plus double-ς were employed in the heavier elements.[19] The geometry optimization of H_2 was carried out at the B3LYP level with a more complete basis set, cc-pVQZ.[26]

Orbital Interactions in Kinetic Energy Density (KED)

Within the Kohn−Sham theory, the "positive" KED is obtained as a summation of the kinetic energy densities of all of the occupied Kohn−Sham orbitals, $\psi_i(\mathbf{r})$[12]

$$t(\mathbf{r}) = \sum_i n_i t_i(\mathbf{r}) = \frac{1}{2}\sum_i n_i \nabla \psi_i^*(\mathbf{r}) \cdot \nabla \psi_i(\mathbf{r})$$

where n_i is the occupation number and $t_i(\mathbf{r})$ is defined as the "orbital KED" for $\psi_i(\mathbf{r})$. The integration of the KED, $t(\mathbf{r})$, in direct space provides the total kinetic energy of the electrons. The Kohn−Sham orbitals can be constructed by various basis functions including plane waves and atomic orbitals. When atomic orbitals are employed, the Kohn−Sham orbitals are constructed as a linear combination of the atomic orbitals, $\chi_\mu(\mathbf{r})$'s

$$\psi_i(\mathbf{r}) = \sum_\mu c_{\mu i}\chi_\mu(\mathbf{r})$$

where $c_{\mu i}$ is the orbital coefficient. The electron density is then obtained as the summation of the electron densities of all of the occupied Kohn−Sham orbitals

$$\rho(\mathbf{r}) = \sum_i n_i \rho_i(\mathbf{r}) = \sum_i n_i \psi_i^*(\mathbf{r})\, \psi_i(\mathbf{r})$$

Here, we recognize a remarkably simple mathematical similarity between the electron density and the KED; the former is from the absolute square of the Kohn−Sham orbitals and the latter is from the absolute scalar square of their gradients. Meanwhile, the well-known, pair-orbital decomposition scheme of the electron density provides the information on how an orbital pair-interaction, for example, between $\chi_\mu(\mathbf{r})$ and $\chi_\upsilon(\mathbf{r})$, contributes to the electron accumulation or depletion in the internuclear region

$$\rho(\mathbf{r}) = \sum_{\mu,v} P_{v\mu} \chi_\mu^*(\mathbf{r})\, \chi_v(\mathbf{r})$$

where $P_{v\mu}$ is the charge density matrix element[27]

$$P_{v\mu} = \sum_i n_i c_{\mu i}^* c_{vi}$$

The spatial integrals of the overlap densities weighted by the density matrix elements lead to the formulation of the orbital overlap population analysis.

From the mathematical similarity between the electron density and the KED, we now recognize that the KED also can be decomposed into pairwise orbital interaction components

$$t(\mathbf{r}) = \frac{1}{2}\sum_{\mu,v} P_{v\mu} \nabla \chi_\mu^*(\mathbf{r}) \cdot \nabla \chi_v(\mathbf{r})$$

In other words, the electron accumulation or depletion (i.e., the bonding or antibonding) resulting from the overlap of an orbital pair is directly associated with the KED component of the orbital pair. To illustrate this, we employ H_2 as an example, for which the bonding and antibonding MOs are constructed as in-phase and out-of-phase combinations of the 1s orbitals, respectively

$$\psi_+ = \frac{\chi_A + \chi_B}{\sqrt{2(1+S)}} \qquad \text{and} \qquad \psi_- = \frac{\chi_A - \chi_B}{\sqrt{2(1-S)}}$$

The corresponding orbital KEDs are given as

$$t_+ = \frac{1}{2(1+S)}(\nabla\chi_A \cdot \nabla\chi_A + 2\,\nabla\chi_A \cdot \nabla\chi_B + \nabla\chi_B \cdot \nabla\chi_B)$$

and

$$t_- = \frac{1}{2(1-S)}(\nabla\chi_A \cdot \nabla\chi_A - 2\,\nabla\chi_A \cdot \nabla\chi_B + \nabla\chi_B \cdot \nabla\chi_B)$$

It is noted that the critical difference is the signs in the interatomic terms, $\nabla\chi_A \cdot \nabla\chi_B/(1+S)$ in the bonding orbital KED and $-\nabla\chi_A \cdot \nabla\chi_B/(1-S)$ in the antibonding orbital. Because these signs are related to the absence/presence of a nodal plane between the two hydrogen atoms for the MOs, it is expected that the orbital KEDs should somehow reflect the nodal properties. Figure 1a,b shows the orbital KED curves (magenta curve) for the bonding and antibonding orbitals along the bond axis.[28] Whereas the on-site contribution (cyan curve) is always positive in Figure 1, it is noted that the interatomic contribution (brown curve) changes its sign along the bond axis; for bonding, it is negative inside the internuclear region and positive outside (the opposite is true for antibonding).[29] The consequence is that in the internuclear region along the bond axis the KED of the bonding MO is lowered from the simple summation of the KEDs of the individual atomic orbitals, whereas it is raised in the outer region. For the antibonding MO, the KED behaves in the opposite way. Much larger KED values are noted for the antibonding MO because of the normalization condition, which is consistent with the known behavior of MO electron densities.

The origin of the observed behavior of the orbital KEDs is rather apparent and interesting. In the internuclear region along the bond axis, the value of the $1s_A$ orbital decreases as the electron moves away from the atomic center of H_A (Figure 1), thereby resulting in a negative $\nabla\chi_A$, but the same movement increases the value of the $1s_B$ orbital (i.e., positive $\nabla\chi_B$) as the electron moves toward the atomic center of H_B. Consequently, $\nabla\chi_A \cdot \nabla\chi_B$ is negative in the internuclear region. $\nabla\chi_A \cdot \nabla\chi_B$ is always positive outside the region because both $\nabla\chi_A$ and $\nabla\chi_B$ have the same sign. In other words, the KED increases as the electron passes through the nodal plane in the antibonding orbital. The electron density is depleted in the nodal plane region as the electrons move faster and do not stay in the region for long. The constructive interference of the atomic orbitals in the bonding orbital reduces the electron kinetic energy in the internuclear region of the bond and thus allows electrodensity to accumulate because of the slowing of the electron.

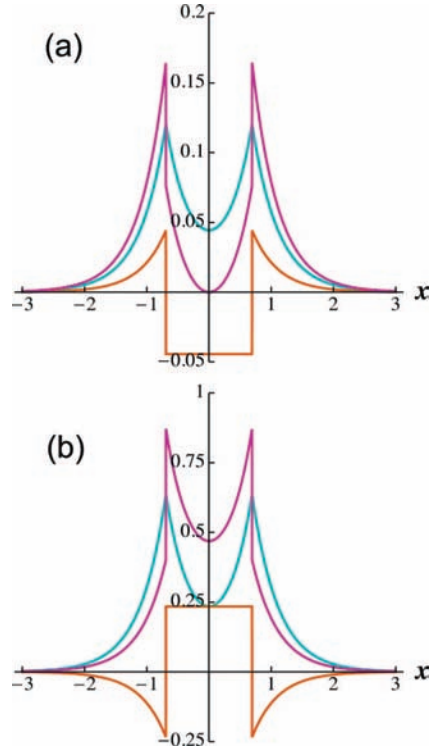

Figure 1. KED plots along the bond axis of H_2 for (a) bonding and (b) antibonding MOs from 1s STOs. The total contribution is magenta, the on-site contribution is cyan, and the the interatomic contribution is brown. Atomic units are employed.

More complicated orbital overlaps will produce more complex patterns of the orbital KED in space, and the patterns of the KED may be analyzed among different compounds for studies of their chemical bonding. The mathematical correlation between the nodal properties and the orbital KED should exist generally for other types of orbital interactions (s−p, p−p, s−d, p−d, and so on). The same is true even for the nodal planes or spheres of individual atomic orbitals themselves, which will be discussed in a separate publication. Furthermore, when atomic orbitals are orthogonal, they do not contribute to the total kinetic energy, which is also a necessary feature for a suitable bonding descriptor.

Figure 2a,b shows the elevation maps of the KED calculated for a longitudinal cross section of the H_2 molecule with two and four electrons, respectively. With two electrons in the bonding MO, Figure 2a shows a decrease in the KED from the internuclear region, as expected from Figure 1a. The KED increases rapidly as the electrons move closer to the nuclear positions (the apical positions) and decreases less prominently when the electrons are moving away from the internuclear region. With two additional electrons occupying the antibonding MO, the calculated KED in Figure 2b is significantly larger in the internuclear region and decreases rapidly in the outer region. This behavior is close to what we expect for the KED of the antibonding MOs, which is understandable when we recognize their much larger KED compared with the KED of the bonding MO (Figure 1a vs b).

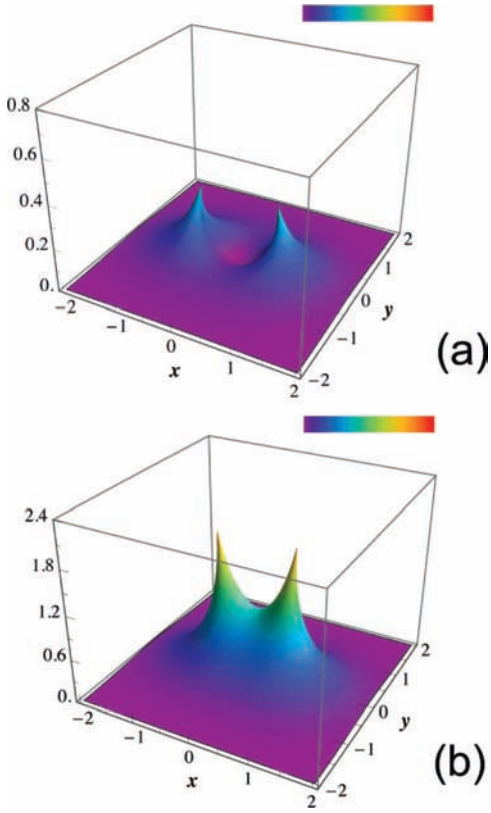

Figure 2. Elevation maps of the KED in a longitudinal cross section containing the bond axis of H_2 for the occupancies of (a) two electrons in the bonding MO and (b) four electrons, two in the bonding MO and two in the antibonding MO from 1s STOs. Atomic units are employed.

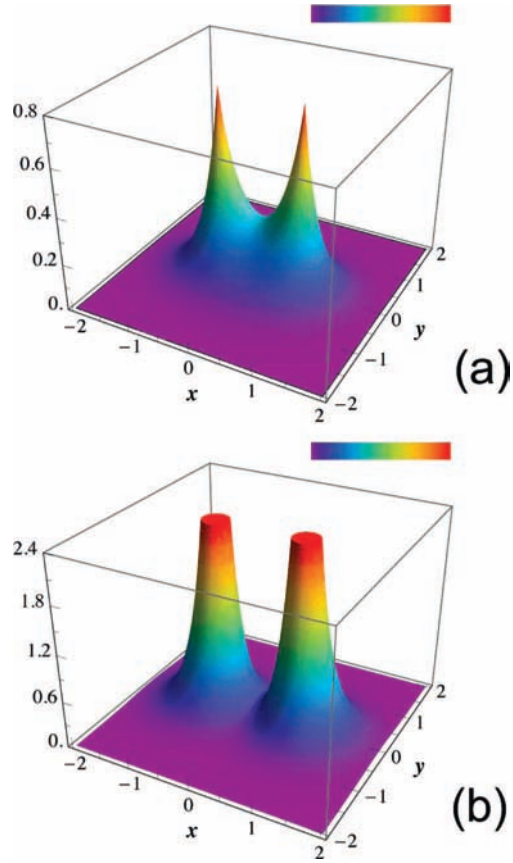

Figure 3. Elevation maps of the TF-KED in a longitudinal cross section containing the bond axis of H_2 for the occupancies of (a) two electrons in the bonding MO and (b) four electrons, two in the bonding MO and two in the antibonding MO from 1s STOs. Atomic units are employed.

Thomas−Fermi Kinetic Energy Density (TF-KED)

From the previous discussions, it is clear that the KED can be interpreted on the basis of orbital interactions for chemical bonding analysis. However, the KED has the same problem that the electron density has; that is, the KED is largest close to the nuclei rather than in the internuclear region, so the subtle deformation of the KED upon chemical bond formation may not be clearly differentiated among different compounds. This problem is partially resolved in the previous studies of the KED by a comparison of the KED of compounds with the KEDs of individual constituent atoms that are calculated separately.[9d] In other words, the direct-space map of the superimposed atomic KEDs can serve as a reference for examining the spatial variations of the KED of the compounds. Because we are more interested in the bonding analysis from single calculations for given compounds, however, we pursue a different approach. We utilize the TF-KED as our reference because it contains the major part of the KED that can be readily obtained from the electron density.[30] Indeed, serious efforts have been devoted to finding better models of the KED by adding smaller components to the TF-KED as the starting point.[31]

The aforementioned orbital interpretation of the KED is useful in contrasting the nature of the TF-KED with the chemical point of view. As the simplest approximate form of the KED, the TF-KED is obtained by assuming that the electrons feel only a constant electrical potential (free electron or jellium model).[32]

$$t_{TF}(\mathbf{r}) = \frac{3}{10}(3\pi^2)^{2/3}\rho^{5/3}(\mathbf{r})$$

From the equation, the TF-KED is an increasing function of the electron density; that is, any electron accumulation in space produces a larger TF-KED value at the position. This is a direct consequence of the free electron approximation in the Thomas−Fermi theory. In the free electron model, there is an infinite number of continuous energy levels whose relative positions are determined solely by their kinetic energy component. For an electron density value at a position in a real system, such as an atom or a compound, we then imagine a hypothetical free electron system that has the same density that is constant throughout the chemical structure. The Thomas−Fermi theory simply takes the uniform kinetic energy of the hypothetical system as an approximate KED (TF-KED) at the specific position in the real system. The increase in the electron density means that the electrons further populate the higher-energy levels, hence resulting in larger TF-KED values. As described previously, however, proper KEDs behave more or less in the opposite way. When the electron density deforms because of chemical bond formation, the electron accumulation (depletion) in the interatomic region is associated with the lowering (increasing) of the KED in the region as a result of the nodal properties. The same contrasting behaviors are expected at the nodal planes of individual atomic orbitals. The unreasonable characteristic of the TF-KED is not inconsistent with the well-known Teller's molecular nonbinding theorem that states the implausibility of the TF-KED as the correct KED for any molecular system.[14] For our purpose, the contrasting behaviors of the TF-KED and the KED should be beneficial when we examine the chemical bonding in the internuclear regions.

Figure 3a,b presents the elevation maps of the TF-KED that correspond to the KED maps in Figures 2a,b, respectively. In

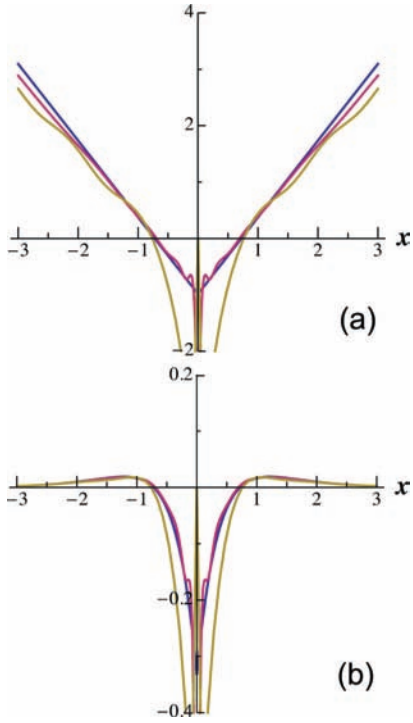

Figure 4. (a) ARED and (b) RED plots across the nucleus of an H atom. Dark-blue curves are algebraically from 1s STOs, purple curves are from the Gaussian 03 program, and brown curves are from the VASP calculations. Atomic units are employed.

Figure 3a, the rise of the TF-KED is clearly seen in the internuclear region where the electron density builds up in the bonding MO density. In the same region, the electron accumulation in the bonding MO and the electron depletion in the antibonding MO compensate for each other so that there is no relatively significant deformation of the TF-KED around the nuclei when the H_2 has four electrons (Figure 3b).

Relative Entropy Density (RED)

A mere comparison between the TF-KED and the KED will remain obscure in chemical bonding analysis because the total electronic energy change upon bonding, which includes both kinetic and potential energy components, matters most. However, a quantitative comparison is indeed possible when we employ the relative entropy defined by Nagy and Parr.[12] The relative entropy is the difference between the entropy functional, S, and the corresponding Thomas−Fermi entropy, S_{TF}, within the local density functional theory

$$S - S_{TF} = \frac{3}{2}k\int d\mathbf{r}\ \rho(\mathbf{r}) \ln \frac{t(\mathbf{r})}{t_{TF}(\mathbf{r})}$$

where k is the Boltzmann constant. It is noted that the integral contains the ratio of the KED and the TF-KED in a natural logarithmic form multiplied by the electron density. The entropy functional and the Thomas−Fermi entropy are the integrals of the entropy density, $s(\mathbf{r})$, and the Thomas−Fermi entropy density, $s_{TF}(\mathbf{r})$

$$s(\mathbf{r}) = \frac{3}{2}k\rho(\mathbf{r}) \ln \frac{t(\mathbf{r})}{t_{TF}(\mathbf{r})} + s_{TF}(\mathbf{r})$$

and

$$s_{TF}(\mathbf{r}) = \frac{3}{2}k\rho(\mathbf{r})$$

The Thomas−Fermi entropy is defined as the model entropy functional obtained by approximating the KED to be the TF-KED, and thus, it is given as $3kN/2$, in which N is the total number of electrons.

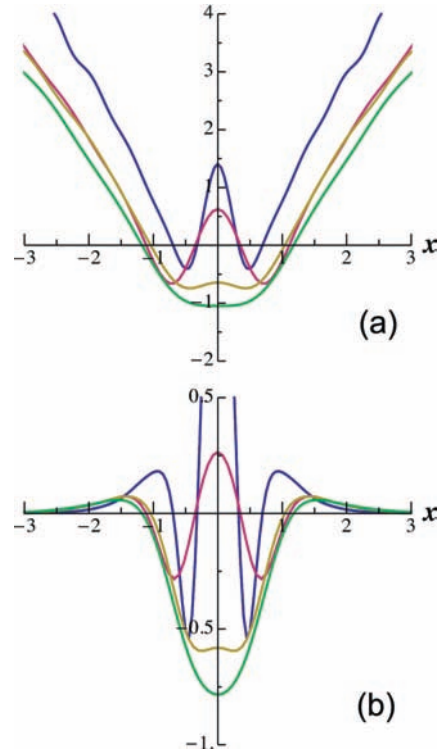

Figure 5. (a) ARED and (b) RED plots across the nucleus of C (dark blue), Si (purple), Ge (brown), and α-Sn (dark green) atoms, obtained from the VASP calculations. The x axis is in angstroms. The ARED has no units, and the RED is in angstroms^{-3}.

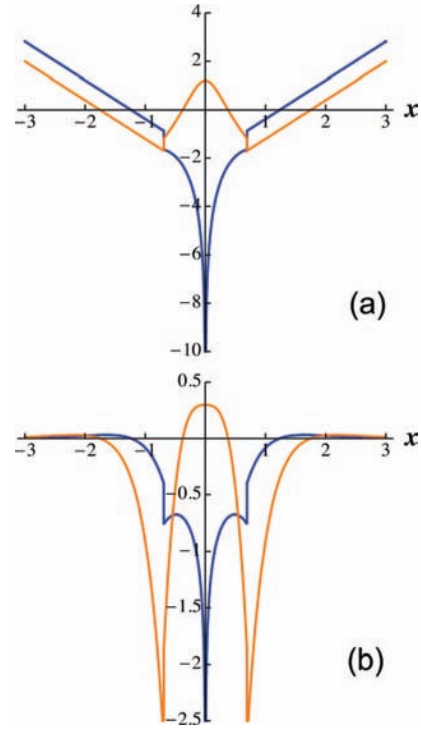

Figure 6. (a) ARED and (b) RED plots along the bond axis of H_2 algebraically from 1s STOs. The blue curves are for the occupancy of two electrons in the bonding MO, and the orange curves are for four electrons, two in the bonding MO and two in the antibonding MO. Atomic units are employed. The kinks at the nuclear positions are due to the cusp condition.

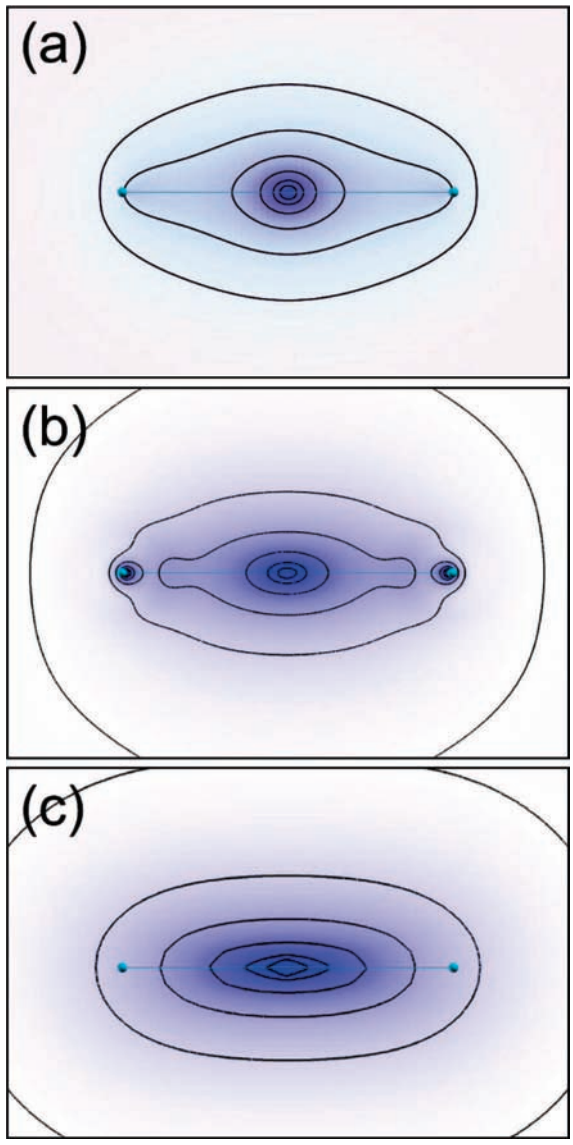

Figure 7. RED contour maps in a longitudinal cross section containing the bond axis of an H_2 molecule (a) from 1s STOs, (b) from the Gaussian 03 program, and (c) from the VASP calculations. The most intense blue color, around the center of the bond, corresponds to -13.5 Å^{-3}, and the contour interval is 2.7 Å^{-3} after the first contour from the center. The white color corresponds to zero. The slightly different colors in part a are due to the differences between the Mathmatica 6 graphic utilities and the XCrysDen program.

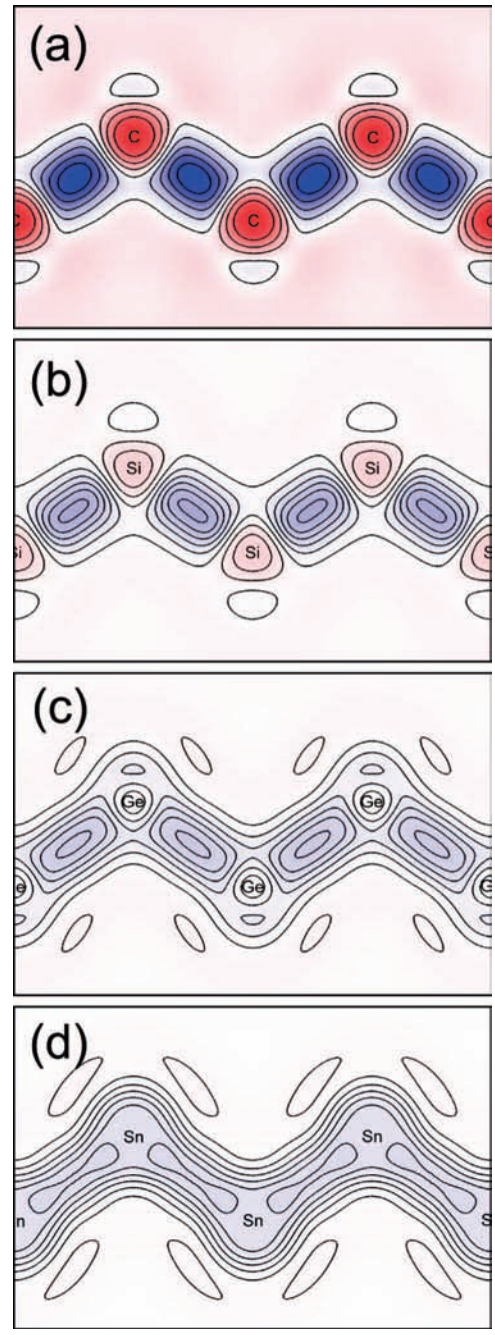

Figure 8. RED contour maps for the (110) cross section containing (a) C−C, (b) Si−Si, (c) Ge−Ge, and (d) Sn−Sn bonds in the elements, from the VASP calculations. The contour intervals are (a) 0.50, (b) 0.17, (c) 0.10, and (d) 0.07 Å^{-3}, and the minimum RED values are given in Table 1. All of the Figures use the same color scheme with the most intense blue color in (a) corresponding to -2.48 Å^{-3}. The white color corresponds to zero.

Importantly, the entropy of a system has a maximum value under the same condition that produces a minimum value for the electronic energy (a variation principle called the Nagy−Parr theorem hereafter).

$$\delta^2 S < 0$$

Because the total number of electrons does not change when atoms form a compound, the S_{TF} is constant no matter what electron density the compound has.[12] Therefore, the relative entropy also follows a variation principle

$$\delta^2 (S - S_{TF}) < 0$$

It states that under the Nagy−Parr theorem the TF-KED is a unique reference for the KED in that their corresponding entropy values are maximally different when the system has a minimum electronic energy. Through Teller's molecular nonbinding theorem, the TF-KED is desirable as a special reference that shows no chemical bonding effect even though it is constructed from the electron density of the real system that is already formed by chemical bonding.

For a variationally meaningful comparison between the KED and the TF-KED in direct space, therefore, we define a direct space function called the relative entropy density (RED).

$$\sigma(\mathbf{r}) = \frac{3}{2k}[s(\mathbf{r}) - s_{TF}(\mathbf{r})] = \rho(\mathbf{r}) \ln \frac{t(\mathbf{r})}{t_{TF}(\mathbf{r})}$$

The prefactor $3/2k$ is multiplied in the first equation for the sake of convenience, particularly when the RED is compared

TABLE 1: Minimum RED Values and the Bond Distances for the Solids and Molecules

RED from VASP		bond distance (Å) for VASP calc.[a]	RED from Gaussian 03	bond distance (Å) from Gaussian 03
C−C	−2.48	1.545	−2.10	1.556
Si−Si	−0.874	2.352	−0.775	2.355
Ge−Ge	−0.525	2.450	−0.587	2.491
Sn−Sn	−0.368	2.810	−0.425	2.841
B−N	−1.88	1.566	−1.21	1.614
Al−N	−1.35	1.880	−0.763	1.983
Al−P	−0.872	2.365	−0.612	2.518
Al−As	−0.677	2.442	−0.553	2.619
Al−Sb	−0.486	2.654	−0.425	2.818
Ga−N	−1.28	1.931	−0.756	2.006
Ga−P	−0.845	2.360	−0.616	2.514
Ga−As	−0.645	2.448	−0.560	2.611
Ga−Sb	−0.426	2.640	−0.433	2.806
In−N	−1.12	2.136	−0.676	2.183
In−P	−0.725	2.532	−0.571	2.676
In−As	−0.593	2.623	−0.521	2.772
In−Sb	−0.382	2.806	−0.400	2.971

[a] The bond distances are calculated from the unit cell parameters in refs 35 and 36. It was found that the RED maps and values did not change significantly by the slight unit cell differences in the literature.

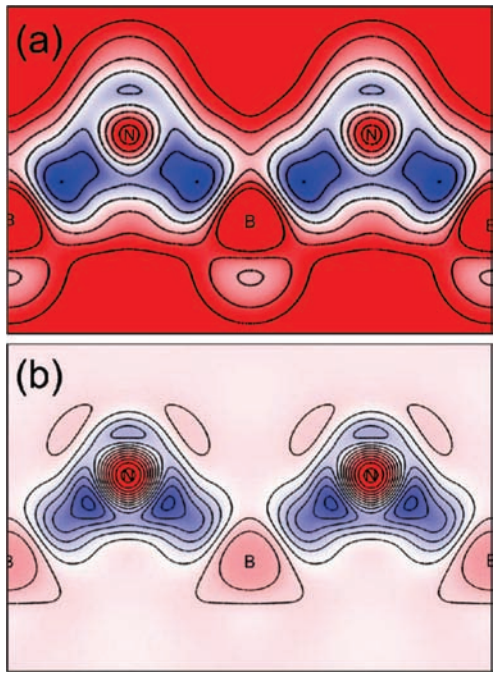

Figure 9. (a) ARED and (b) RED contour maps for the (110) bond cross section of the zinc-blende-type BN from the VASP calculations. In part a, the plot range is from −1.01 to 1.01 with the contour interval of 0.34. In part b, the contour interval is 0.35 Å^{-3}, and the minimum RED value is −1.88 Å^{-3} (Table 1). In part b, the color scheme follows that of Figure 8.

with the electron density map. The ratio between the RED and the electron density provides the RED value per single electron, which we call the average relative entropy density (ARED).

$$\bar{\sigma}(\mathbf{r}) = \ln \frac{t(\mathbf{r})}{t_{\mathrm{TF}}(\mathbf{r})}$$

In Figure 4a,b, the dark-blue curves show the radial dependence of the ARED and the RED of an isolated H atom with one electron occupying the Slater-type 1s orbital (1s STO) with the orbital exponent $\varsigma = 1$ (in atomic units). The ARED is positive when a single electron is far from the nucleus, and it decreases linearly as the electron comes closer to the nucleus and becomes bound to it. It is reiterated that the ARED essentially represents the relative value of the KED with respect to the TF-KED. The negative value of the ARED indicates that the KED of the electron is lower than what we expect from the free electron model at this position, which is reasonable for the bound state of the electron. The RED curve, the electron-density-weighted ARED, shows the same behavior, but the value decreases far from the nucleus (Figure 4b).

The striking linear behavior of the ARED is due to the exponential dependence of the radial component of the 1s STO; in fact, the slope is calculated algebraically as $4\varsigma/3$ in atomic units. The ARED and RED curves are more complex for the orbitals in the upper shells because of the orthogonalization condition. However, we find that for the radial part of any single-ς orbitals the slope of the ARED approaches $4\varsigma/3$ asymptotically away from the nucleus, whether they are hydrogenlike or Slater-type, and this result can be utilized as a reference for the ab initio or first principle calculation results.[33] The purple and brown curves in Figure 4 are obtained for the hydrogen atom from Gaussian 03 and VASP calculations, respectively. The two methods are distinctly different so that the generality of the new functions can be examined to a great extent. For the inner part of the atom in Figure 4, both the ARED and RED curves are drastically different among the three data sets because of their disparate ways of constructing the basis functions. However, it is important that they are similar in the outer region where the chemical bonding takes place. In Figure 4a, the numerical results are indeed consistent with the algebraic result that is from the ideal ς value of 1 for the 1s STO of the hydrogen atom. The variational ς value of 1.197 for H_2 in Figures 1 and 2 is much larger than 1, which is due to the orbital contraction upon bond formation.

The oscillatory behavior of the ARED from the VASP results may be due to the nature of the plane waves that the VASP program employs or simply because of numerical errors, yet the deviation is quite small in the corresponding RED curve. The oscillation is much less in the VASP results for heavier elements, as we can see in Figure 5 where the ARED and RED curves are shown for the valence electrons of isolated C, Si, Ge, and Sn atoms in their hypothetical spin-unpolarized ground state with equally populated p orbitals. All of the ARED curves show linear behavior with positive values in the outer region, whereas they are significantly different in the inner region for different valence shells. For the heavier atoms, the ARED is more or less constant in the inner region. The corresponding RED curves have similar values in the outer region except for the C atom, the lightest in the group. The corresponding calculations were not carried out with the Gaussian 03 program because of its occupation number restriction for open-shell systems. In Figure S1 of the Supporting Information, the RED contour maps are produced from the VASP calculations for all of the atoms in groups 13−15 down to the fifth period.

A comment on the pseudopotential methods is given here before we continue the discussion of our results. In describing atoms by the pseudopotential or effective-core-potential methods, pseudoatomic orbitals are generated by smoothing the inner part (core-penetrating tail) of the atomic orbitals so that they essentially describe only the part of the orbitals that are alterable in bond formation. As far as the KED is concerned, the effect is that a significant portion of the high kinetic energy of the

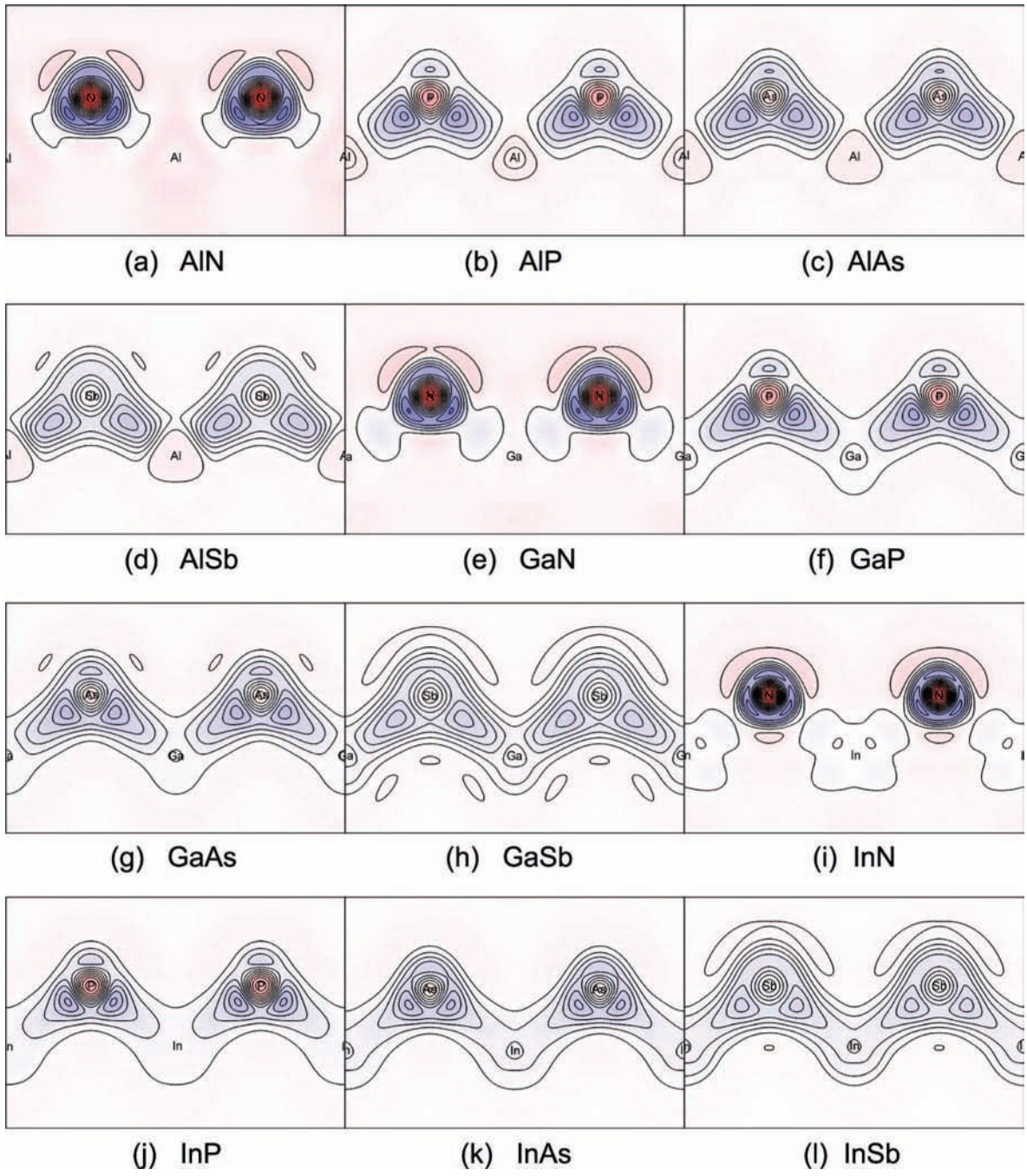

Figure 10. RED contour maps for the (110) bond cross section of binary III−V compounds in the zinc blende structure from the VASP calculations. The contour intervals are (a) 0.25, (b) 0.17, (c) 0.12, (d) 0.09, (e) 0.25, (f) 0.16, (g) 0.12, (h) 0.08, (i) 0.21, (j) 0.14, (k) 0.11, and (l) 0.07 $Å^{-3}$, and the minimum RED values are given in Table 1. For all of the Figures, the color scheme follows that of Figure 8.

orbitals in the inner atomic region is treated essentially as an additional positive electrostatic potential that cancels most of the large negative attractive potential from the nucleus.[9e] Consequently, the kinetic energy of the pseudoatomic orbitals does not change as rapidly close to the nuclei and thus simplifies the ARED and RED maps, as shown later. It is noted that the pseudoatomic orbitals have an electron density that is different from the original atomic orbitals and that in our studies the TF-KED is obtained from this pseudo-orbital density. Such treatment of the TF-KED is not new and can be found in previous applications of the Thomas−Fermi model for molecules in which the effective nuclear charges were employed.[34] In those studies, the exclusion of the core−electron density was found to provide a better utilization of the TF-KED, which is reasonable considering the nature of the free electron model. Much more recently, it has been shown that the kinetic energy from the pseudopotential methods is sound in the studies of chemical bonding mechanisms: covalent bonding, polar charge transfer, and electron correlations, within both ab initio and density functional formalisms.[9e] This is because the pseudopotential methods effectively eliminate complex core effects, simulate the core penetration of the valence electrons, and provide pseudopotentials that recover the chemical similarity and trends in the groups of the periodic table.

When two hydrogen atoms form a molecule, their ARED and RED are affected by the orbital interaction. From the KED and TF-KED of the hydrogen molecule in Figures 1 and 2, the corresponding ARED and RED are drawn respectively in Figure 6a,b for the two different electron occupancies, two and four (in blue and orange). They are also given in the elevation maps

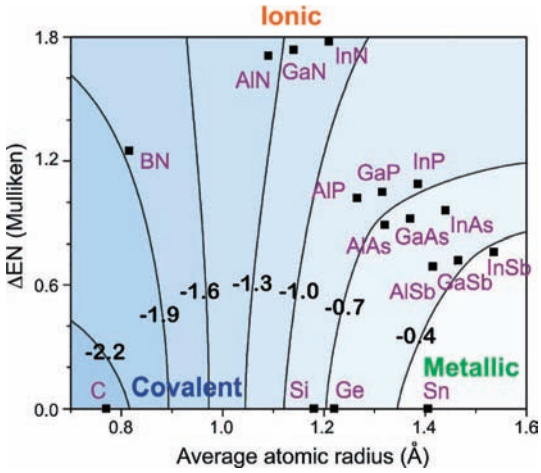

Figure 11. Overlay of the minimum RED values from the VASP in Table 1 on the map of the tetrahedral network solids according to the average atomic radius and Mulliken's electronegativity (EN) difference.[36] The isolines of the minimum RED serve only as crude guidelines. The conventional ionic regime resides beyond the maximum ΔEN on the map.

in the Supporting Information (Figure S2). When only the bonding orbital is filled, both the ARED and RED are lowered in the bonding region compared with the values in the off-bonding region. The lowering is so significant that the values are strongly negative with their minimum at the center of the bond. With both of the bonding and antibonding orbitals being completely filled in a hypothetical case, the ARED and RED values around the bond center are much larger than the values in the off-bonding region. This is consistent with the net antibonding character found for the closed-shell atoms in simple MO theory.

In Figure 7, the RED contour maps are compared for the H_2 molecule from (a) the variational optimization of the 1s STOs (as in Figures 2 and 3), (b) Gaussian 03, and (c) VASP calculations. In the blue-white-red color gradient in the RED maps, a blue color indicates a negative value of the RED (that is, the KED is lower than the TF-KED), whereas a red color indicates the opposite. The color gradient scheme in all of the RED contour maps herein is symmetric so that the most intense blue and red in the color bar always have the same absolute values. The RED maps in Figure 7 are consistent; they all show strongly negative values in the bonding region with the minimum at the bonding center. The maximum values are positive but very close to zero in the comparison (0.206, 0.205, and 0.232 $Å^{-3}$ in a−c, respectively), as represented by an almost-white color off the bonding region. The major difference in the VASP result from the others is that it does not show kinks or ripples around the nuclei because of the pseudopotential treatment of the 1s orbital. The smooth monotonic change in the RED around the nuclei reflects the fact that the pseudo-1s orbitals represent only the alterable part of the electronic motion in the hydrogen atoms.

Metallicity in Chemical Bonding of the Group 14 Elements

We now examine the RED maps of C, Si, Ge, and α-Sn in their diamond structure, especially with respect to how the originally spherically symmetric RED of atoms becomes altered (or deformed) in the bond formation. In addition to the atomic RED curves in Figure 5, we refer to their 2-D cross-sectional views in Figure S1 in the Supporting Information for the

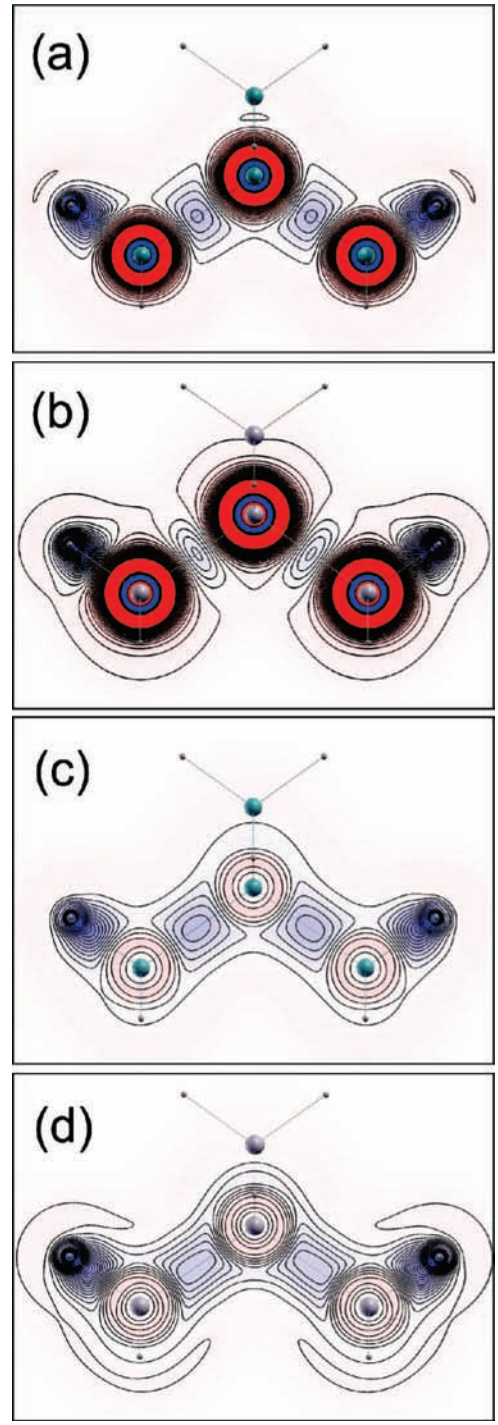

Figure 12. RED contour maps of $Si(SiH_3)_4$, (a) and (c), and $Ge(GeH_3)_4$, (b) and (d), from Gaussian 03 calculations. Parts a and c are from the all-electron calculations at the B3LYP/6-311G level. Parts b and c are obtained from the effective core potential calculation results at the B3LYP/LANL2DZ level. The contour intervals are 0.17 $Å^{-3}$ for parts a and c and 0.10 $Å^{-3}$ for parts b and d. The minimum RED values along the central bonds are −0.698, −0.318, −0.775, and −0.587 $Å^{-3}$ for parts a−d, respectively. The color scheme follows that of Figure 8.

comparison. It is noted that for the lighter atoms, C and Si, the RED is positive in the inner region; that is, the electrons in the pseudoatomic orbitals move faster in the inner region than what is expected from the TF-KED. For the heavier atoms, Ge and Sn, the electrons are slower, giving negative values of the RED, which is the case of the pseudo-1s orbital of the hydrogen atom. For all of the atoms, the outer part of the pseudo-orbitals

shows positive RED values. The RED changes drastically in the bonding region in Figure 8, in which the RED contour maps are given for a cross section in the diamond structures of the elements. In all of the maps, the most intense blue and red are set to −2.48 and 2.48 $Å^{-3}$, respectively, so that the same color intensity corresponds to the same absolute RED value. The lowest RED values (the most intense blue region) are located at the center of the bonds, except for α-Sn. The contour lines show a symmetric shape, and the RED values increase gradually from the center of the bond axis toward two neighboring atoms in the case of C, Si, and Ge. In an ascending order, the minimum RED values are −2.48, −0.874, −0.525, and −0.368 $Å^{-3}$ for C, Si, Ge, and α-Sn (Table 1). The C−C bond is considered to be the strongest bond with the largest negative RED value. The absolute decrease in the minimum RED values for the heavier elements is consistent with their weaker bonding character.

For α-Sn, the heaviest element in Figure 8, the most-negative RED values are spread around each Sn atom rather than at the center of the bonds, and the values are much closer to zero, the free electron limit. In addition, the RED values in the bond region are close to those in the inner region of the Sn atoms. These features reflect the metallic nature of the weak covalent bonding in α-Sn. In essence, the alterable part of the pseudo-atomic orbitals of Sn becomes deformed in such a way that the electrons in those orbitals are more or less freely moving through the nuclear positions. In the case of C, the blue region is strongly localized in the bonding region, indicating a strong nonmetallic behavior, and the electrons are strongly scattered (increase in the KED) by the presence of the nuclei and core electrons in the bonding path. These observations are consistent with the general trend of the orbital interactions among the group elements. Namely, whether a diamond structure of the group 14 elements is insulating or metallic depends on the extent of the s−p hybridization, which is in turn governed by the energy difference between the s and p orbitals and the diffuseness of these orbitals. For the case of a metallic diamond structure, which occurs when the energy and diffuseness are very different between the s and p orbitals, the bonding and antibonding s bands lie below the p bands and are completely filled, hence leading to partially filled p bands. The diffused nature of the p orbitals of the heavier elements and their weak interactions is evident in the overall low negative RED values in Figures S1 and 8. The opposite is true for the case of an insulating diamond structure, and the bottom portion of the conduction bands has substantial s orbital character.

Bond Polarity in the III−V Zinc-Blende-Type Compounds

When electrons are partially transferred from one atom to another during the covalent bond formation, the orbital contraction is more severe for the cationic atom than for the anionic one. In the model studies of H_2^+-like heteronuclear diatomic cations in which each atom has a 1s STO with a different effective nuclear charge, it has been found that the variationally optimized ζ values show a more severe increase from the original value for the atom with a lower nuclear charge (the more electropositive atom, cationic) than for the one with a larger charge (the more electronegative atom, anionic).[8e] Because the slope of the ARED is directly proportional to the ζ, the charge transfer will make the positive ARED region expand around the cationic atom significantly, but that will not be the case around the anionic atom. Certainly, this expansion may become negated along the bonding path by the lowering of the ARED as a result of the covalent bonding component.

The fundamental origin of the ARED changes is the behaviors of the KED and the TF-KED upon charge transfer. The KED increases (decreases) in the inner region as the orbitals contract (expand) because of the charge transfer from the inner (outer) region to the outside (inside). Because the TF-KED is a monotonic function of the electron density, however, it behaves in the opposite way; the decrease (increase) in the electron density in the inner region produces a decrease (increase) in the TF-KED. In any event, the sign of the RED values is strictly determined by the ARED, and hence, the electron transfer from an atom to a more electronegative atom will increase the positive RED area around the former, whereas it may increase or keep the negative area around the latter.

Figure 9a,b shows the ARED and RED maps of BN in a zinc blende structure. In the comparison to the neutral carbon atoms in Figure 8a, the nitrogen atoms in Figure 9b have more significantly negative RED regions, whereas the boron atoms increase the area of the positive region around them. This is consistent with our prediction based on the behavior of the kinetic energy densities. The deep blue regions close to the nitrogen nuclei point toward the neighboring boron atoms, reflecting the directional nature of the B−N bond. The origin of the lowest RED values localized on the nitrogen atoms can be examined by comparing the ARED (Figure 9a) and the RED (Figure 9b) maps. In Figure 9a, the modulation of the ARED is much stronger around the boron atoms than the nitrogen, as more intense blue and red colors coexist around the boron. The electron transfer from the boron atom to the nitrogen raises the ARED to more positive values, but around the B−N bonding axis, this effect is overridden by the covalent bonding formation. Although not shown here, this is observed in general for the other polar bonds and the electron transfer appears to modify the ARED more on the cationic sites than on the anionic sites. When the ARED is weighted with the electron density to produce the RED, however, the most negative RED values become localized around the anionic sites because of the higher valence electron density.

When the electronegativity difference becomes larger, the covalency of the bond decreases, and the bond becomes more polar. Compared with the BN, the RED map of the AlN (Figure 10a) shows much more localized negative regions around the nitrogen atoms. The relatively spherical symmetry of the RED values around both aluminum and nitrogen atoms suggests a relatively strong ionic bonding character. With the decrease in the electronegativity difference in AlN to AlSb down group 15, the deepest-blue region moves toward the center of the bond, and the colors become gradually less intense (Figure 10a−d). The minimum RED values from the VASP calculations are −1.35, −0.872, −0.677, and −0.486 $Å^{-3}$ for AlN, AlP, AlAs, and AlSb, respectively, as shown in Table 1, indicating a stronger metallicity for the heavier elements. For the comparison, the RED values were calculated from the Gaussian 03 program by employing geometry-optimized molecular anions, $X(YH_3)_4^{3-}$, in which the group 15 atom, X, is tetrahedrally bonded to four Y atoms (group 13) that are saturated by an additional three hydrogen atoms. The RED maps for the X−Y bond cross section are shown in Figure S3 in the Supporting Information. Despite the fact that our Gaussian 03 calculations employ the discrete molecular models, the VASP and Gaussian 03 results are consistent, showing the same trend in the minimum RED values except for the slightly opposite behavior between AlSb and GaSb. The RED values from the Gaussian 03 calculations are found to be somewhat smaller in magnitude than those from

the VASP. More significant deviations for the nitrides in Table 1 will be explained in the next section.

The RED trend in the aluminum compounds is found also for the gallium and indium compounds (Figure 10e−l). For both GaN and InN, the minimum RED values are more strongly localized, and the RED distribution is more symmetrical around the nitrogen atoms compared with AlN, which is consistent with the electronegativity trend giving a higher bond polarity in GaN and InN. The indium atoms in the InN show a broad but weakly negative RED region around the nuclei, and it is reminiscent of the metallic character of the Sn (Figure 10i). The InSb shows the strongest metallicity overall with the least-intense colors while still displaying the bond polarity between the In and Sb atoms.

In Figure 11, the minimum RED values from the VASP calculations are plotted for the tetrahedral network solids according to the average atomic radius and the Mulliken electronegativity difference.[37] Overall, the trend of the RED values is consistent with the commonly expected bond metallicity. The minimum RED values decrease in negative with the increase in the average atomic radius so that the covalent bond strength decreases. It is noted in Figure 11 that the minimum RED values range widely among different polar bonds, and hence the RED values may not be an indicator of bond polarity. Rather, the bond polarity affects the deformation of the atomic RED upon the bond formation, as described in the previous discussions. The more significantly the eletronegativities are different, the more the atomic RED deforms around the cationic sites and the more strongly the minimum RED positions shift to the anionic sites.

Pseudopotential versus All-Electron Methods

As previously mentioned, the RED can be calculated with only the valence electrons, especially through the pseudopotential methods, which is preferred in our implementation of the RED concept. However, this approach contrasts the observation in the studies of ELF in that the inclusion of the core electrons leads to more reasonable values.[5e] Therefore, we make a comparison of the Gaussian 03 results from the effective core potential (pseudopotential) and the all-electron methods using, as an example, the $Si(SiH_3)_4$ and $Ge(GeH_3)_4$ compounds in which the central atom is tetrahedrally bonded to four identical atoms (isostructural to the $X(YH_4)_3^{3-}$ anions in the previous section). In Figure 12a,b, the RED maps are shown for the silicon and germanium compounds, respectively, from all-electron calculation results. The inner part of the heavy atoms shows an apparent ring structure with very strong undulations of the RED because of the core electrons. Because the core electron region overlaps significantly with the valence part, the RED values in the bonding region are severely affected by the core electron contribution, particularly for the germanium analogue.

In the RED maps from the Gaussian 03 pseudopotential calculation results (Figure 12c,d), a contrasting feature is that the effect of the bond formation by the valence electrons is clearly seen even in the close proximity of the nuclei. In the pseudopotential results, the minimum RED values are −0.775 and −0.587 $Å^{-3}$ at the center of the bond for the silicon and germanium compounds, respectively (Table 1). Being far from the nuclei, those values are still significantly reduced to −0.698 and −0.318 $Å^{-3}$ in the all-electron results because of the interfering positive contribution from the core electrons. These observations embellish the advantage of the pseudopotential method for the utilization of the RED concept in addition to the computational efficiency of the method for heavy elements. The carbon analogue is not discussed here because the LANL2DZ basis set, or any others in the Gaussian 03 program, includes core orbitals (full potential) for the first and second period elements. However, the all-electron result for the carbon analogue is close to the outcome of the VASP calculations (Table 1), indicating that the core electrons are highly localized in the inner region and do not affect the RED values significantly in the internuclear region. However, the deviation becomes significant when the negative RED region is highly localized close to the more electronegative atoms such as in all of the nitrides in Table 1.

Concluding Remarks

Whereas the spatial distribution of the variationally obtained kinetic energy (or the KED in this work) has been recognized as an essential representation of the chemical bonding, it is striking to note that the mathematical structure of the KED inherently allows its interpretation on the basis of the orbital interactions even at the level of one-electron theory. The elemental components for the interpretation are both the quantitative manifestation of the nodal properties of the orbitals by the KED and the intrinsic composition of the KED from the pairwise orbital interactions through the density matrix. The TF-KED from the free electron model contrasts the KED because its predicted behavior is opposite to that of the KED as a result of its relationship with the electron density. Upon our utilizing the Nagy−Parr theorem, an algebraic combination of the electron density, the KED, and the TF-KED produces a variationally meaningful direct space function, RED, that can differentiate divergent types of chemical bonding with different degrees of metallicity and polarity, as demonstrated in this work. This initial success warrants more extensive applications and an examination of the RED function in the studies of chemical bonding, which are under way in our current research, especially on challenging electronic systems such as intermetallics, metal hydrides, and Zintl-border compounds.

Acknowledgment. D.-K.S. is grateful for financial support from the National Science Foundation through his CAREER Award (DMR contract no. 0239837) and from the Camille and Henry Dreyfus Foundation for his Camille Dreyfus Teacher-Scholar Award. D.-K.S. thanks Professor Yuri Grin for introducing him to the benefits of chemical bonding analysis in direct space and acknowledges stimulating discussions with Professor Ulrich Häussermann and Drs. Miroslav Kohout and Frank Wagner.

Supporting Information Available: Complete ref 19; contour of the RED for atoms in groups 13−15; elevation of the ARED and the RED for an H_2 molecule with two different electron occupancies; contour of the RED for $C(CH_3)_4$, $Si(SiH_3)_4$, $Ge(GeH_3)_4$, $Sn(SnH_3)_4$, and $X(YH_3)_4^{3-}$ from the effective core potential Gaussian 03 calculations. This material is available free of charge via the Internet at http://pubs.acs.org.

References and Notes

(1) See, for example, (a) Burdett, J. K. *Chemical Bonding in Solids*; Oxford University Press: New York, 1995. (b) Nesper, R. *Angew. Chem., Int. Ed.* **1991**, *30*, 789.

(2) Hughbanks, T.; Hoffmann, R. *J. Am. Chem. Soc.* **1983**, *105*, 3528.

(3) Dronskowski, R.; Blöchl, P. E. *J. Phys. Chem.* **1993**, *97*, 8617.

(4) Bader, R. F. W. *Atoms in Molecules: A Quantum Theory*; Oxford University Press: New York, 1994.

(5) (a) Becke, A. D.; Edgecombe, K. E. *J. Chem. Phys.* **1990**, *92*, 5397. (b) Savin, A.; Jepsen, O.; Flad, J.; Andersen, O. K.; Preuss, H.; Von

Schnering, H. G. *Angew. Chem., Int. Ed.* **1992**, *31*, 187. (c) Silvi, B.; Savin, A. *Nature* **1994**, *371*, 683. (d) Burdett, J. K.; McCormick, T. A. *J. Phys. Chem. A* **1998**, *102*, 6366. (e) Kohout, M.; Savin, A. *J. Comput. Chem.* **1997**, *18*, 1431.

(6) (a) Kohout, M.; Pernal, K.; Wagner, F. R.; Grin, Y. *Theor. Chem. Acc.* **2004**, *112*, 453. (b) Kohout, M.; Pernal, K.; Wagner, F. R.; Grin, Y. *Theor. Chem. Acc.* **2005**, *113*, 287. (c) Wagner, F. R.; Bezugly, V.; Kohout, M.; Grin, Y. *Chem.—Eur. J.* **2007**, *13*, 5724.

(7) (a) Schmider, H. L.; Becke, A. D. *THEOCHEM* **2000**, *527*, 51. (b) Schmider, H. L.; Becke, A. D. *J. Chem. Phys.* **2002**, *116*, 3184.

(8) (a) Ruedenberg, K. *Rev. Mod. Phys.* **1962**, *34*, 326. (b) Rue, R. R.; Ruedenberg, K. *J. Phys. Chem.* **1964**, *68*, 1676. (c) Feinberg, M. J.; Ruedenberg, K.; Mehler, E. L. *Adv. Quantum Chem.* **1970**, *5*, 27. (d) Feinberg, M. J.; Ruedenberg, K. *J. Chem. Phys.* **1971**, *54*, 1495. (e) Feinberg, M. J.; Ruedenberg, K. *J. Chem. Phys.* **1971**, *55*, 5804.

(9) (a) Kutzelnigg, W. *Angew. Chem., Int. Ed.* **1973**, *12*, 546. (b) Kutzelnigg, W. *Einführung in die Theoretische Chemie*;Verlag: Weinheim, Germany, 1978; *Vol. 2*, Section 3.3. (c) Kutzelnigg, W. The Physical Origin of the Chemical Bond. In *The Concept of the Chemical Bond*; Maksic, Z. B., Ed.; Springer-Verlag: Berlin, Germany, 1990. (d) Ruedenberg, K.; Schmidt, M. W. *J. Comput. Chem.* **2007**, *28*, 391. (e) Bitter, T.; Ruedenberg, K.; Schwarz, W. H. E. *J. Comput. Chem.* **2007**, *28*, 411.

(10) Perdew, J. P.; Kurth, S. Density Functionals for Non-Relativistic Coulumb Systems in the New Century. In *A Primer in Density Functional Theory*; Fiolhais, C., Nogueira, F., Marques, M., Eds.; Springer: New York, 2003, and references therein.

(11) Chattaraj, P. K.; Chamorro, E.; Fuentealba, P. *Chem. Phys. Lett.* **1999**, *314*, 114.

(12) Nagy, A.; Parr, R. G. *THEOCHEM* **2000**, *501−502*, 101.

(13) (a) Ghosh, S. K.; Berkowitz, M.; Parr, R. G. *Proc. Natl. Acad. Sci. U.S.A.* **1984**, *81*, 8028. (b) Nagy, A.; Parr, R. G.; Liu, S. *Phys. Rev. A* **1996**, *53*, 3117.

(14) (a) Teller, E. *Rev. Mod. Phys.* **1962**, *34*, 627. (b) Balazs, N. L. *Phys. Rev.* **1967**, *156*, 42. (c) Lieb, E. H.; Simon, B. *Phys. Rev. Lett.* **1973**, *31*, 681. (d) Lieb, E. H.; Simon, B. *Adv. Math.* **1977**, *23*, 22. (e) Spruch, L. *Rev. Mod. Phys.* **1991**, *63*, 1512.

(15) (a) Baerends, E. J.; Gritsenko, O. V. *J. Phys. Chem. A* **1997**, *101*, 5383. (b) Stowasser, R.; Hoffmann, R. *J. Am. Chem. Soc.* **1999**, *121*, 3414.

(16) Seo, D.-K. *J. Chem. Phys.* **2006**, *125*, 154105. (b) Seo, D.-K. *J. Chem. Phys.* **2007**, *127*, 184103.

(17) Kohout, M. *D-Grid*; Max-Planck-Institut für Chemische Physik fester Stoffe: Dresden, Germany, 2005.

(18) (a) Kresse, G.; Hafner, J. *Phys. Rev. B* **1993**, *47*, 558. (b) Kresse, G.; Hafner, J. *Phys. Rev. B* **1994**, *49*, 14251. (c) Kresse, G.; Furthmüller, J. *Comput. Mater. Sci.* **1996**, *6*, 15. (d) Kresse, G.; Furthmüller, J. *Phys. Rev. B* **1996**, *54*, 111169.

(19) Frisch, M. J.; Trucks, G. W.; Schlegel, H. B.; Scuseria, G. E.; Robb, M. A.; Cheeseman, J. R.; Montgomery, J. A., Jr.; Vreven, T.; Kudin, K. N.; Burant, J. C.; Millam, J. M.; Iyengar, S. S.; Tomasi, J.; Barone, V.; Mennucci, B.; Cossi, M.; Scalmani, G.; Rega, N.; Petersson, G. A.; Nakatsuji, H.; Hada, M.; Ehara, M.; Toyota, K.; Fukuda, R.; Hasegawa, J.; Ishida, M.; Nakajima, T.; Honda, Y.; Kitao, O.; Nakai, H.; Klene, M.; Li, X.; Knox, J. E.; Hratchian, H. P.; Cross, J. B.; Bakken, V.; Adamo, C.; Jaramillo, J.; Gomperts, R.; Stratmann, R. E.; Yazyev, O.; Austin, A. J.; Cammi, R.; Pomelli, C.; Ochterski, J. W.; Ayala, P. Y.; Morokuma, K.; Voth, G. A.; Salvador, P.; Dannenberg, J. J.; Zakrzewski, V. G.; Dapprich, S.; Daniels, A. D.; Strain, M. C.; Farkas, O.; Malick, D. K.; Rabuck, A. D.; Raghavachari, K.; Foresman, J. B.; Ortiz, J. V.; Cui, Q.; Baboul, A. G.; Clifford, S.; Cioslowski, J.; Stefanov, B. B.; Liu, G.; Liashenko, A.; Piskorz, P.; Komaromi, I.; Martin, R. L.; Fox, D. J.; Keith, T.; Al-Laham, M. A.; Peng, C. Y.; Nanayakkara, A.; Challacombe, M.; Gill, P. M. W.; Johnson, B.; Chen, W.; Wong, M. W.; Gonzalez, C.; Pople, J. A. *Gaussian 03*, revision C.02; Gaussian, Inc.: Wallingford, CT, 2004.

(20) Kokalj, A. *J. Mol. Graphics Modell.* **1999**, *17*, 176.

(21) (a) Blöchl, P. E. *Phys. Rev. B* **1994**, *50*, 17953. (b) Kresse, G.; Joubert, D. *Phys. Rev. B* **1999**, *59*, 1758.

(22) (a) Perdew, J. P.; Chevary, J. A.; Vosko, S. H.; Jackson, K. A.; Pederson, M. R.; Singh, D. J.; Fiolhais, C. *Phys. Rev. B* **1992**, *46*, 6671. (b) Perdew, J. P.; Chevary, J. A.; Vosko, S. H.; Jackson, K. A.; Pederson, M. R.; Singh, D. J.; Fiolhais, C. *Phys. Rev. B: Condens. Matter Mater. Phys.* **1993**, *48*, 4978.

(23) Becke, A. D. *J. Chem. Phys.* **1993**, *98*, 5648.

(24) Lee, C.; Yang, W.; Parr, R. G. *Phys. Rev. B* **1988**, *37*, 785.

(25) Hay, P. J.; Wadt, W. R. *J. Chem. Phys.* **1985**, *82*, 270.

(26) Dunning, T. H., Jr *J. Chem. Phys.* **1989**, *90*, 1007.

(27) Szabo, A.; Ostlund, N. S.; Section 3.4.3. *Modern Quantum Chemistry: Introduction to Advanced Electronic Structure Theory*; McGraw-Hill: New York, 1989.

(28) We employ a Slater-type 1s orbital (1s STO) optimized variationally in H_2 with $\chi(\mathbf{r}) = (\zeta^3\pi)^{-1/2} \exp(-\zeta\mathbf{r})$, $\zeta = 1.197$. See, for example, Levine, I. N. *Quantum Chemistry*, 4th ed.; Prentice Hall: Englewood Cliffs, NJ, 1991; Section 13.9.

(29) The discontinuity of the orbital KEDs at the nuclear positions originates from the cusp condition of the atomic orbitals.

(30) The same approach was taken for the development of the LOL (ref 5).

(31) Parr, R. G.; Yang, W. *Density-Functional Theory of Atoms and Molecules*; Oxford University Press: New York, 1989; Chapter 6.

(32) (a) Thomas, L. H. *Proc. Cambridge Philos. Soc.* **1927**, *23*, 542. (b) Fermi, E. *Rend. Accad. Naz. Lincei* **1927**, *6*, 602. (c) Fermi, E. *Z. Phys.* **1928**, *48*, 73. (d) March, N. H. *Adv. Phys.* **1957**, *6*, 1. (e) March, N. H. *Self-Consistent Fields in Atoms: Hartree and Thomas−Fermi Atoms*; Pergamon: New York, 1975.

(33) The y-intercept is given as $\ln(\pi^{2/3}/2c_F)$ ($=-0.985$), where $c_F = 3/10(3\pi^2)^{2/3}$ for the 1s STOs (in atomic units). It also depends on the occupancy and normalization factors for the case of MOs.

(34) (a) Buckingham, R. A.; Massay, H. S. W.; Tibbs, S. R. *Proc. R. Soc. London, Ser. A* **1941**, *178*, 119. (b) Coulson, C. A.; March, N. H. *Proc. Phys. Soc. A* **1950**, *63*, 367. (c) Coulson, C. A.; March, N. H. *Proc. Cambridge Philos. Soc.* **1956**, *52*, 114. (d) Banyard, K. E.; March, N. H. *Acta Crystallogr.* **1956**, *9*, 385. (e) Banyard, K. E.; March, N. H. *Proc. Cambridge Philos. Soc.* **1956**, *52*, 280.

(35) *ICSD (Inorganic Crystal Structure Database)*; Fachinformationszentrum Karlsruhe (FIZ), Germany, and the National Institute of Standards and Technology (NIST), 2007.

(36) Madelung, O. *Semiconductor: Data Handbook*; Springer: New York, 2004.

(37) Huheey, J. E.; Keiter, E. A.; Keiter, R. L. *Inorganic Chemistry: Principles of Structure and Reactivity*, 4th ed.; Prentice Hall: Englewood Cliffs, NJ, 1997.

JP803279E